

Dilatometric characteristics of weakly sintered ceramics

Yury I. Komolikhov ^a, Larisa V. Ermakova ^{b*} , Vladimir R. Khrustov ^c,
Victor D. Zhuravlev ^b 

a: M.N. Mikheev Institute of Metal Physics, Ural Branch of the Russian Academy of Sciences, Ekaterinburg 620108, Russia

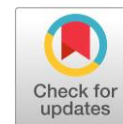
b: Institute of Solid State Chemistry, Ural Branch of the Russian Academy of Sciences, Ekaterinburg 620990, Russia

c: Institute of Electrophysics, Ural Branch of the Russian Academy of Sciences, Ekaterinburg 620016, Russia

* Corresponding author: larisaer@ihim.uran.ru

This paper belongs to a Regular Issue.

© 2022, the Authors. This article is published in open access under the terms and conditions of the Creative Commons Attribution (CC BY) license (<http://creativecommons.org/licenses/by/4.0/>).



Abstract

Thermal expansion of refractory ceramics CaZrO_3 , MgAl_2O_4 , $\text{La}_2\text{Zr}_2\text{O}_7$ and YSZ-12 was studied. The samples of the complex oxides were synthesized by solution combustion synthesis with glycine; the fuel:oxidant ratio was varied depending on the character of redox reaction. The linear thermal expansion coefficient (LTEC) of ceramics was measured on the samples with an initial density 23–52%. The maximal sinterability of 89–92% after 6 h annealing at 1550 °C was demonstrated by $\text{La}_2\text{Zr}_2\text{O}_7$ and YSZ-12, and the minimal values (78–82%) – by CaZrO_3 and MgAl_2O_4 . All materials have close LTEC values, from 9.0 to $9.6 \cdot 10^{-6} \text{ K}^{-1}$.

Keywords

refractory oxide
weakly sintered ceramics
linear thermal expansion coefficient
thermal expansion
ceramic density

Received: 29.06.22

Revised: 25.08.22

Accepted: 01.09.22

Available online: 13.09.22

1. Introduction

Thermal stability of ceramic materials based on zirconium and/or aluminum oxides makes it possible to use them as functional ceramics and thermal barrier coatings at high temperatures [1–5]. However, under the action of high temperatures, especially during abrupt heating or cooling, internal stresses appear in the material – usually compression stresses, tensile stresses of cut, and more rarely bending stresses. As a result, cracks are formed in ceramics or coatings leading to their destruction. The number and the value of stresses depend on the elastic properties and thermal expansion of anisotropic phases and/or crystals in ceramics [6, 7]. For thermal barrier coatings (TBC) it is particularly important to determine the linear thermal-expansion coefficient (LTEC), since for providing good contact between layers of gradient coating it is necessary to select compositions with close, gradually varying LTEC values. This prevents cracking or exfoliation of coating from the substrate in the process of thermal cycling [8–10].

The most widespread methods of TBC application are: 1) kinds of plasma spraying: Atmospheric Plasma Spraying (APS), Low-pressure Plasma Spray (LPPS), Solution Precursor Plasma Sprayed (SPPS); 2) Chemical Vapor Deposition (CVD); 3) Chemical Gas-dynamic Spraying (CGDS) [11–15]. Of much interest is the sol-gel procedure allowing one to

apply coatings on complex-shaped articles (as distinct from APS and Electron Beam Vacuum Plasma Deposition (EB-PVD)), as well as multilayer coatings. Besides, its cost is comparable with the cost of production of coatings by the APS method [16, 17].

The principle of this method consists in the formation of a coating from a deposit as a result of hydrolysis (pyrolysis, thermolysis, combustion of polymer-salt composition, xerogel). The temperature of coating formation from oxide powder depends on the temperature at which initial salts and components decompose in this technique. Then the coating is heat treated and sintered at chosen temperatures. The key controlled parameter affecting the characteristics (porosity, homogeneity, thickness) and quality of coating is the rate of oxide coating formation from gel (xerogel).

However, the initial density of coating in these technologies is much lower than that for materials produced with the use of plasma methods. As a result, such processes as formation of crystal phases, coarsening and sintering of crystallites, inevitable emergence of structural defects, cracking, etc., take place in coatings during the high-temperature treatment. For successful development of this coating method it is necessary to study the behavior of low-density and porous ceramics during sintering. Therefore, the aim of this work is to perform dilatometric studies of weakly sintered refractory materials CaZrO_3 , MgAl_2O_4 ,

$\text{La}_2\text{Zr}_2\text{O}_7$ and ZrO_2 -12 produced by Solution Combustion Synthesis (SCS) [18–21].

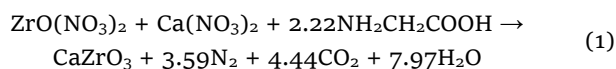
2. Experimental

2.1. Starting materials

Zirconium and calcium carbonates, magnesium, lanthanum and yttrium oxides, aluminum nitrate nonahydrate, nitric acid, glycine were used as initial reagents. Metal carbonates and oxides were preliminarily dissolved in nitric acid. The resulting solutions were mixed in the required stoichiometric amount, and powders of CaZrO_3 , MgAl_2O_4 , $\text{La}_2\text{Zr}_2\text{O}_7$ and ZrO_2 -12 mol.% Y_2O_3 were produced by Solution Combustion Synthesis. The powders were prepared in a wide aluminum reactor with a capacity of 3 dm³. To reduce heat removal, the reactor had asbestos sheet insulation. Other conditions for the production of samples are given below. The sample of CaZrO_3 prepared at the Donetsk plant of chemical reagents (DPCR) was used as a reference.

2.2. Preparation of CaZrO_3

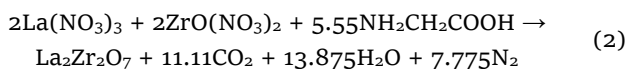
CaZrO_3 was synthesized at $\varphi = 1.0$ in accordance with equation 1, i.e. stoichiometric ratio of fuel and oxidizer, which ensures the maximum speed and temperature of the SCS process [22]:



SCS reaction under stoichiometric conditions ($\varphi = 1.0$) leads to complete oxidation of organic fuel (glycine), the precursors are white in color (Figure 1a). The produced CaZrO_3 powders were mixed, placed in corundum crucibles and annealed in a muffle furnace at a temperature of 1100 °C for 5 h to complete the crystallization. Upon annealing, the product decreased in volume by 5–10%.

2.3. Preparation of $\text{La}_2\text{Zr}_2\text{O}_7$

Synthesis was performed from a solution of lanthanum and zirconyl nitrates containing 160 g/dm³ of precursors expressed as $\text{La}_2\text{Zr}_2\text{O}_7$ with glycine ($\varphi = 1.0$) according to equation 2:



Due to a large amount of gases evolved during the reaction, the precursor takes the shape of foam or whipped cream, which decreases the degree of particle sintering. The precursor was mixed and annealed in corundum crucibles for 5 h at 900 °C. The annealed product was averaged by way of short-term agitation.

2.4. Preparation of MgAl_2O_4

Aluminum-magnesium spinel was synthesized by equation 3 in oxidative regime ($\varphi = 0.6$) [22] from a solution of magnesium and aluminum nitrates containing 67 g/dm³ or precursors expressed as MgAl_2O_4 .

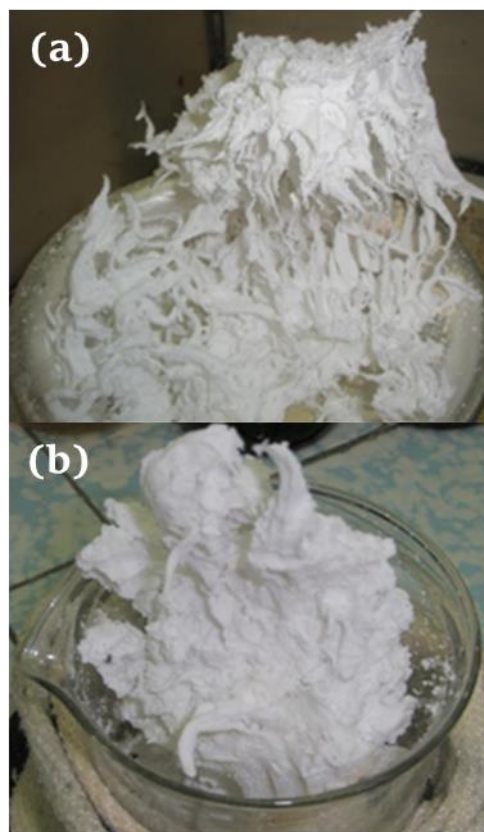
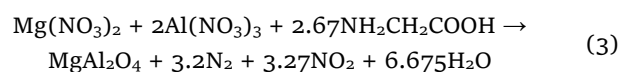


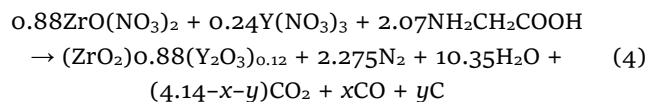
Figure 1 Appearance of CaZrO_3 (a) and $\text{La}_2\text{Zr}_2\text{O}_7$ (b) powders after SCS ($\varphi = 1.0$).



This synthesis regime was chosen to reduce the rate of combustion and prevent the removal of the material outside the reactor. Upon completion of combustion, a downy powder of light brown color was formed. The precursor was annealed at 850 °C for 5 h. The product annealed at 850 °C was ground and additionally annealed at 900 °C for 5 h.

2.5. Preparation of YSZ-12

The powder was synthesized by reaction 4 with a considerable excess of glycine ($\varphi = 1.52$) by calcining the solution of yttrium and zirconyl nitrates containing 128.5 g/dm³ of precursors expressed as YSZ-12.



Since the SCS reaction occurs in the reduction combustion regime, the produced downy and voluminous powder has a gray-brown color due to carbon impurity remaining in the synthesis product as a result of incomplete oxidation of carbon atoms in glycine. The content of unburnt carbon was not estimated; that is why the quantities of the carbon-containing components in equation 4 are given as variables x and y . Upon annealing in air at 900 °C, the powder became white. In order to complete the reaction of synthesis, the material was ground and annealed for 5 h at 1100 °C with subsequent grinding.

2.6. Sample preparation procedure for measurement of LTEC

For the preparation of molding material, each produced powder with a preassigned composition was further mechanically activated with addition of PVC as a binder [23]. The samples for measurements were molded by semidry uniaxial static pressing under a pressure of 160 MPa and preliminarily sintered at 1000 °C. The ceramics for investigation was represented by cylinders of $d = 4.5 \pm 0.2$ mm in diameter and $l = 10.0 \pm 0.2$ mm in length. The opposite faces of the cylinders were made plane-parallel, the distance between faces (l_0) was fixed before the experiment.

2.7. Research methods

The X-ray diffraction studied were performed on a Shimadzu XRD-7000 X-ray diffractometer in Cu K α radiation ($\lambda = 1.5456$ Å) in the 2θ angle interval from 10 to 70° in stepwise scanning mode with $\Delta(2\theta) = 0.03^\circ$ and exposition of 3 s. The determination of the phase composition, structure refinement and coherent scattering region (CSR) definition were carried out using the ICDD and ICSD files and WINXPOW and POWDER CELL 2.4 programs.

The structural and morphological characteristics were studied on a JEOL JSM 6390 LA scanning electron microscope. The specific surface of the powders was determined by the BET method (Tri Star 3000V6.03A) from thermal desorption of nitrogen. The density of the sintered ceramics was determined by hydrostatic weighing in alcohol on a Shimadzu AUW-220 D balance equipped with a special attachment.

The linear thermal expansion of ceramic samples was studied on a Dilatometer DIL 402 C (NETZSCH, Germany). Heating to 1550 °C was carried out with a constant rate of 5 °C/min; simultaneously, air blowing at a rate of 100 cm³/h provided constant atmosphere and a uniform temperature field. The samples were cooled with the furnace to room temperature. The results of dilatometric studies were used to calculate the integral (average) LTEC (α_{av}) in the temperature interval ($T_1 - T_0$) (equation 5):

$$\alpha_{av} = \frac{1}{L_0} \cdot \frac{(L_1 - L_0)}{(T_1 - T_0)}, \quad (5)$$

where L_0, L_1 are initial and final length of the sample; T_0, T_1 are initial and final temperature, respectively. The dimensional accuracy (ΔL) was 0.133%; it was determined by the nonlinearity of the dilatometer displacement meter transfer function.

3. Results and discussion

In combustion reactions, fine-dispersed oxide precursor is formed as a result of decomposition of metalorganic complexes [23]. Generous and rapid gas liberation promotes the formation of high-porous, chemically non-equilibrium powders with a small bulk weight and low density. Usually, these are bulk powders composed of aggregates of nano- and microparticles (Figures 2, 3). Aggregates of powders, for example CaZrO₃, practically do not sinter at temperatures up to 900–1000 °C without preliminary grinding. After mechanical activation (long-term grinding), the original CaZrO₃ aggregates are partially destroyed and form more dense, albeit more fine, in comparison with the powders obtained by the solid-phase method (Figure 2).

The morphology of aluminum-magnesium spinel upon annealing at 900 °C differs from other materials and is represented by denser particle aggregates, although less dense than for CaZrO₃ produced by the solid-phase method (Figure 4).

All samples after SCS are mixed-phase materials, and the morphological features of the powders allow their active sintering to be carried out at lower temperatures. In the process of high-temperature annealing, the samples become single-phase. The crystal-chemical characteristics of the examined materials are listed in Table 1.

The densities of the samples after sintering at 1550 °C for 2 h (dilatometer) and 6 h (muffle furnace) are shown in Table 2. In the former case, sintering was performed in a dilatometer with measurement of the sample length variation, in the latter case – in a chamber furnace; the heating in all cases was carried out at a rate of 5 °C/min. The obtained results indicate that the density of the samples is practically independent of the holding time of ceramics at 1550 °C.

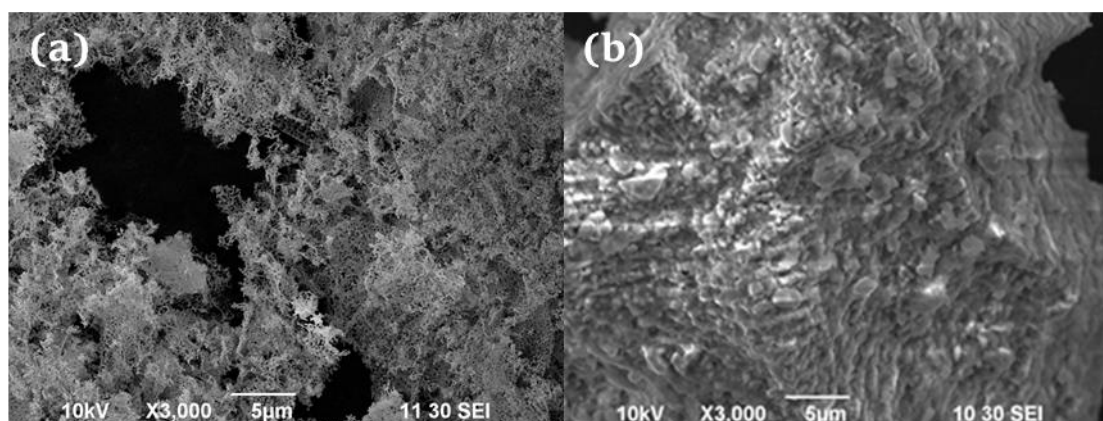


Figure 2 Morphology of CaZrO₃ powder produced by SCS method (a) and at DPCR (b).

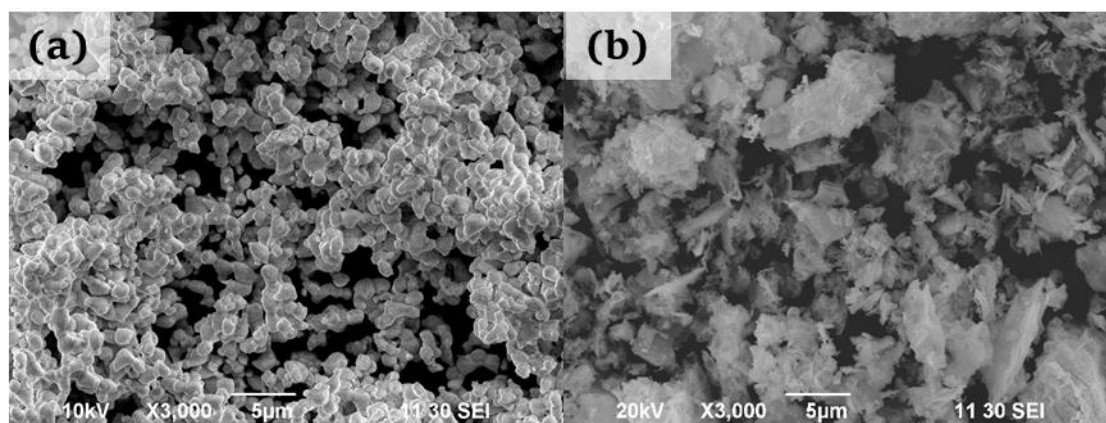


Figure 3 Morphology of $\text{La}_2\text{Zr}_2\text{O}_7$ (a) and YSZ-12 powders (b).

Table 1 Physicochemical characteristics of powders.

Sample	Structure	Phase composition	Unit cell parameters, Å	CSR, nm
CaZrO_3	Pbnm	Traces of ZrO_2 cub.	5.753 ± 0.001	114 ± 1
CaZrO_3 (DPCR)	Pbnm	CaZrO_3 68.9%	–	–
MgAl_2O_4	Fd-3m	100%	8.083 ± 0.001	18 ± 1
$\text{La}_2\text{Zr}_2\text{O}_7$	Fd-3m	100%	10.763 ± 0.001	21 ± 1
YSZ-12	Fm-3m	100%	5.145 ± 0.001	90 ± 1

Note that the initial density of MgAl_2O_4 and $\text{La}_2\text{Zr}_2\text{O}_7$ samples did not exceed 30% of the theoretical one. Upon 2 h annealing at 1550 °C both CaZrO_3 samples exhibited moderately high density values, 76–77%; approximately the same density values were observed for the MgAl_2O_4 sample (Table 2). The sample of $\text{La}_2\text{Zr}_2\text{O}_7$ ceramic had the maximal value of density, 98%.

Three-fold enhancement of the annealing time, from two to six hours, did not lead to any considerable increase in density (Table 2). This effect is likely to be due to stronger sintering inside powder aggregates of these materials and the absence of diffusion processes between particle aggregates [24].

Dilatometric analysis of thermal shrinkage makes it possible to trace the regularities and specific features of the examined compacts. Figure 5 displays the temperature dependences of shrinkage during heating to 1550 °C at a rate of 5 °C/min, and Figure 6 – the time dependences allowing one to estimate the effect of isothermal exposure on shrinkage at 1550 °C.

From Figure 5 it is seen that all materials begin to sinter actively at a temperature slightly above 1100 °C. The exception is provided by CaZrO_3 samples of both types (curves 1 and 2). They are characterized by a higher initial sintering temperature, about 1200 °C. Probably, in this way the effect of preliminary annealing of powders performed at elevated temperature manifests itself, leading to coarsening and densification of agglomerates. The maximal shrinkage rate is typical of lanthanum zirconate and magnesium aluminate. The degree of shrinkage of these materials exceeds the limits of the instrument operating range (50%). Therefore, the above-mentioned curves are extrapolated up to the maximal temperature of the experiment.

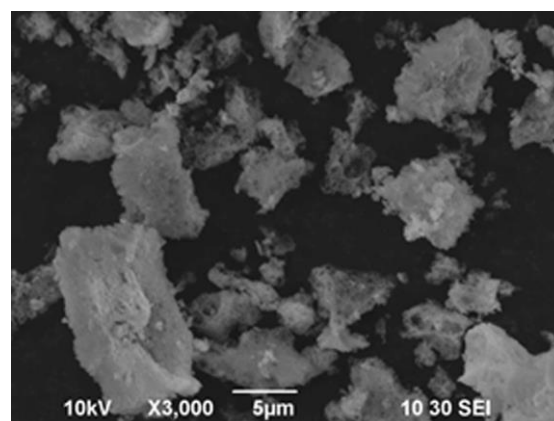


Figure 4 Morphology of MgAl_2O_4 powder upon annealing at 900 °C.

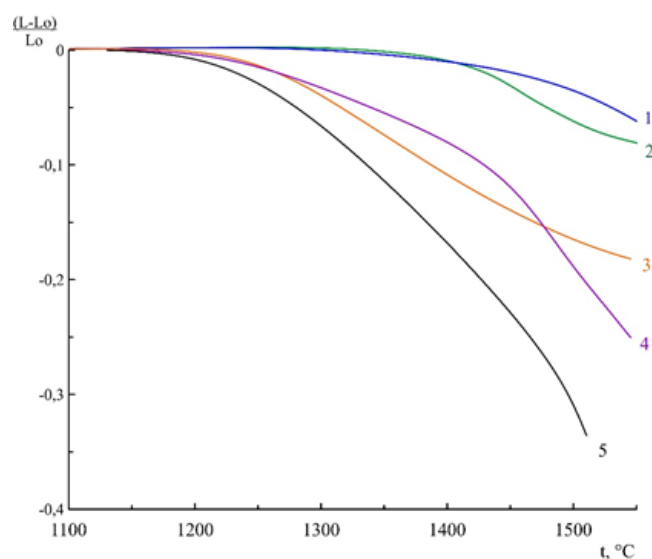
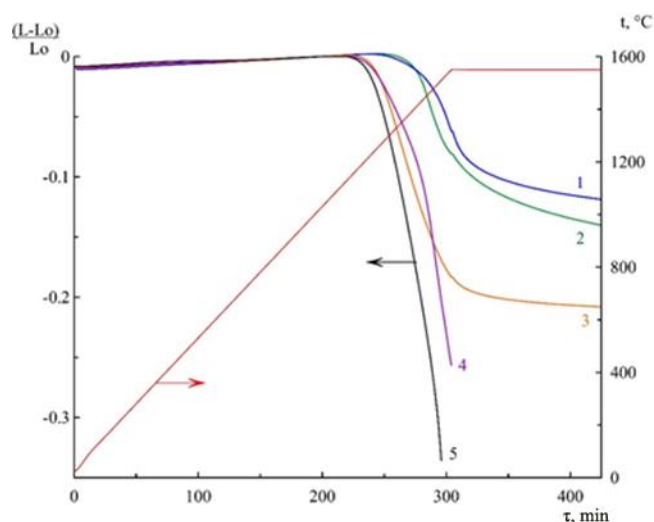


Figure 5 Dilatometric curves during heating at a constant rate of 5 °C/min with isothermal exposure of 2 h at 1550 °C. 1 – CaZrO_3 (SCS); 2 – CaZrO_3 (DPCR); 3 – YSZ-12; 4 – MgAl_2O_4 ; 5 – $\text{La}_2\text{Zr}_2\text{O}_7$.

Table 2 Theoretical, $\rho_{(\text{theor})}$, initial, $\rho_{(\text{init})}$, densities of samples after pressing and preliminary sintering at 1000 °C, and final, $\rho_{(1550)}$, density of samples after annealing at 1550 °C and LTEC values.

Sample	Material	$\rho_{(\text{theor})}$, g/cm ³	$\rho_{(\text{init})}$, g/cm ³ / (%)	$\rho_{(1550)}$, g/cm ³ / (%)		LTEC, 10 ⁻⁶ K ⁻¹
				2 h	6 h	
1	CaZrO ₃ CS	4.78	2.495/(52)	3.626/(76)	3.713/(78)	9.2
2	CaZrO ₃ , DPCR	4.78	2.418/(51)	3.693/(77)	3.781/(81)	9.2
3	YSZ-12	5.90	2.585/(44)	5.378/(91)	5.24/(89)	9.0
4	MgAl ₂ O ₄	4.10	0.987/(29)	2.785/(80)	2.833/(82)	9.6
5	La ₂ Zr ₂ O ₇	6.06	1.397/(23)	5.915/(98)	5.924/(98)	9.3

**Figure 6** A time dependences of the relative linear shrinkage $(L-L_0)/L_0$ in the heating mode at a rate of 5 °C/min to a temperature of 1550 °C, followed by holding for 2 hours: 1 – CaZrO₃ (SCS); 2 – CaZrO₃ (DPCR); 3 – YSZ-12; 4 – MgAl₂O₄; 5 – La₂Zr₂O₇.

The change in the shrinkage of materials with the time of isothermal holding at 1550 °C can be traced from the curves in Figure 6. The nonzero slope of the dilatometric curves during isothermal exposure in the range of 304–424 min indicates that the sintering process of the three materials CaZrO₃ (CS), CaZrO₃ (DPCR), and YSZ-12 is far from completion. An increase in the annealing time did not give a noticeable result: the final density of the three materials was less than 80%, and the density of the YSZ-12 sample even decreased (Table 2). This effect can be associated with significant agglomeration of powders and their internal sintering, since in this case closed pores are formed that prevent compaction [24].

Based on the fact that very loose aggregates of materials with a low initial density were obtained in combustion reactions, the reasons for differences in density after sintering can be (in descending order of probability): 1) the formation of closed porosity; 2) the strength of the formed aggregates of complex oxides; 3) different melting points of the compounds. Possible ways to solve the problem of obtaining denser ceramics may include: 1) lowering the SCS temperature; 2) lowering the degree of agglomeration of powders after synthesis; 3) annealing at a temperature below 1000 °C to avoid reaching chemical equilibrium so as to obtain multiple-phase powders.

4. Conclusions

The effect of weak preliminary sintering (to 23–52% density) on the production and subsequent sintering of dense oxide ceramics CaZrO₃, YSZ-12, MgAl₂O₄ and La₂Zr₂O₇ was studied. It was established that weakly sintered ceramics MgAl₂O₄ and La₂Zr₂O₇ demonstrate continuous shrinkage during annealing in the region of 1100–1550 °C reaching 98% of the theoretical density of ceramics. Preliminary annealing at 1100 °C adversely affects the degree of shrinkage of CaZrO₃ and YSZ-12 compacts leading to coarsening and densification of particle agglomerates.

Supplementary materials

No supplementary materials are available.

Funding

This study was carried out in the framework of the state assignment for the Institute of Solid State Chemistry UB RAS (No. AAAA-A19-119031890026-6), Mikheev Institute of Metal Physics UB RAS (No. AAAA-A18-118020690196-3) and the Institute of Electrophysics UB RAS (No. 122011200363-9).

Acknowledgments

None.

Author contributions

Conceptualization: Yu.I.K., V.D.Zh.
 Data curation: V.D.Zh.
 Formal Analysis: Yu.I.K., V.R.Kh., L.V.E.
 Funding acquisition: V.D.Zh.
 Investigation: V.R.Kh., L.V.E.
 Methodology: Yu.I.K., V.R.Kh., L.V.E.
 Project administration: V.D.Zh.
 Resources: Yu.I.K., V.R.Kh., L.V.E., V.D.Zh.
 Software: L.V.E.
 Supervision: V.D.Zh.
 Validation: Yu.I.K., V.D.Zh.
 Visualization: V.R.Kh., Yu.I.K.
 Writing – original draft: Yu.I.K., V.D.Zh.
 Writing – review & editing: V.D.Zh., L.V.E.

Conflict of interest

The authors declare no conflict of interest.

Additional information

Author IDs:

Yury I. Komolikhov, Scopus ID [6602000371](https://orcid.org/0000-0002-6602-0003);
 Larisa V. Ermakova, Scopus ID [35886395200](https://orcid.org/0000-0001-3588-6395);
 Vladimir R. Khrustov, Scopus ID [6602908178](https://orcid.org/0000-0001-6602-9081);
 Victor D. Zhuravlev, Scopus ID [7202032601](https://orcid.org/0000-0001-7202-0326).

Websites:

M.N. Mikheev Institute of Metal Physics,
<https://www.imp.uran.ru>;
 Institute of Solid State Chemistry, <http://www.solid.nsc.ru>;
 Institute of Electrophysics, <http://eng.iep.uran.ru>.

References

- Zhu D, Miller RA. Development of Advanced Low Conductivity Thermal Barrier Coatings. *Int J Appl Ceram Technol*. 2004;1(1):86–94. doi:[10.1111/j.1744-7402.2004.tb00158.x](https://doi.org/10.1111/j.1744-7402.2004.tb00158.x)
- Yang F, Zhao X, Xiao P. Thermal conductivities of YSZ/Al₂O₃ composites. *J Eur Ceram Soc*. 2010;30(15):3111–3116. doi:[10.1016/j.jeurceramsoc.2010.07.007](https://doi.org/10.1016/j.jeurceramsoc.2010.07.007)
- Shen Z, He L, Xu Zh, Mu R, Huang G. Rare earth oxides stabilized La₂Zr₂O₇ TBCs: EB-PVD, thermal conductivity and thermal cycling life. *Surf Coat Technol*. 2019;357:427–432. doi:[10.1016/j.surfcoat.2018.10.045](https://doi.org/10.1016/j.surfcoat.2018.10.045)
- Lyagaeva YG, Medvedev DA, Demin AK, Yaroslavtseva TV, Plaksin SV, Porotnikova NM. Specific features of preparation of dense ceramic based on barium zirconate. *Semiconductors*. 2014;48(10):1353–1358. doi:[10.1134/S1063782614100182](https://doi.org/10.1134/S1063782614100182)
- Shahbazi H, Tataei M. A novel technique of gel-casting for producing dense ceramics of spinel (MgAl₂O₄). *Ceram Int*. 2019;45(A7):8727–8733. doi:[10.1016/j.ceramint.2019.01.196](https://doi.org/10.1016/j.ceramint.2019.01.196)
- Lyagaeva YG, Medvedev DA, Demin AK, Tsiakaras P, Reznitskikh OG. Thermal expansion of materials in the barium cerate-zirconate system. *Phys Solid State*. 2015;7(2):285–289. doi:[10.1134/S1063783415020250](https://doi.org/10.1134/S1063783415020250)
- Mohanraju S, Ramesha CM, Appaiah S, Kumar J, Krishna Prasad NJ. A study on the impact of coefficient of thermal expansion of Thermo-mechanical stresses on structural components. *Mater Today Proc*. 2021;46(7):2528–2533. doi:[10.1016/j.matpr.2021.01.756](https://doi.org/10.1016/j.matpr.2021.01.756)
- Mobasherpour I, Solati Hashjin M, Razavi Toosi SS, Darvishi Kamachali R. Effect of the addition ZrO₂-Al₂O₃ on nanocrystalline hydroxyapatite bending strength and fracture toughness. *Ceram Int*. 2009;35(4):1569–1574. doi:[10.1016/j.ceramint.2008.08.017](https://doi.org/10.1016/j.ceramint.2008.08.017)
- Yu QM, Cen L. Residual stress distribution along interfaces in thermal barrier coating system under thermal cycles. *Ceram Int*. 2017;43(3):3089–3100. doi:[10.1016/j.ceramint.2016.11.119](https://doi.org/10.1016/j.ceramint.2016.11.119)
- Lim LY, Meguid SA. Thermomechanical simulations of the transient coupled effect of thermal cycling and oxidation on residual stresses in thermal barrier coatings. *Ceram Int*. 2022;48(3):3133–3147. doi:[10.1016/j.ceramint.2021.10.087](https://doi.org/10.1016/j.ceramint.2021.10.087)
- Wei Z-Y, Cai H-N, Zhao S-D. Study on spalling mechanism of APS thermal barrier coatings considering surface vertical crack evolution affected by surrounding cracks. *Ceram Int*. 2022;48(8):11445–11455. doi:[10.1016/j.ceramint.2022.01.001](https://doi.org/10.1016/j.ceramint.2022.01.001)
- Hutsaylyuk V, Student M, Zadorozhna Kh, Student O, Veselivska H, Gvosdetskii V, Maruschak P, Pokhmurska H. Improvement of wear resistance of aluminum alloy by HVOF method. *J Mater Res Technol*. 2020;9(6):16367–16377. doi:[10.1016/j.jmrt.2020.11.102](https://doi.org/10.1016/j.jmrt.2020.11.102)
- Góral M, Swadźba R, Kubaszek T. TEM investigations of TGO formation during cyclic oxidation in two- and three-layered Thermal Barrier Coatings produced using LPPS, CVD and PS-PVD methods. *Surf Coat Technol*. 2020;394:125875. doi:[10.1016/j.surfcoat.2020.125875](https://doi.org/10.1016/j.surfcoat.2020.125875)
- Ma D, Harvey TJ, Zhuk YN, Wellman RG, Wood RJK. Cavitation erosion performance of CVD W/WC coatings. *Wear*. 2020;452–453:203276. doi:[10.1016/j.wear.2020.203276](https://doi.org/10.1016/j.wear.2020.203276)
- Karaoglanli AC, Ozgurluk Y, Doleker KM. Comparison of microstructure and oxidation behavior of CoNiCrAlY coatings produced by APS, SSAPS, D-gun, HVOF and CGDS techniques. *Vacuum*. 2020;180:109609. doi:[10.1016/j.vacuum.2020.109609](https://doi.org/10.1016/j.vacuum.2020.109609)
- Grishina EP, Kudryakova NO, Ramenskaya LM. Thin-film Al₂O₃ coating on low carbon steel obtained by the sol-gel method with different peptizing acids: Corrosion investigation. *Thin Solid Films*. 2022;746:139125. doi:[10.1016/j.tsf.2022.139125](https://doi.org/10.1016/j.tsf.2022.139125)
- Gallyamova R, Galyshev S, Musin F. Preparation of barrier SiO₂ coating on carbon fibers by the sol-gel method. *Mater Today Proc*. 2019;11(1):286–289. doi:[10.1016/j.matpr.2018.12.145](https://doi.org/10.1016/j.matpr.2018.12.145)
- Deganello F, Tyagi AK. Solution combustion synthesis, energy and environment: Best parameters for better materials. *Prog. Cryst. Growth Charact Mater*. 2018;64(2):23–61. doi:[10.1016/j.pcrysgrow.2018.03.001](https://doi.org/10.1016/j.pcrysgrow.2018.03.001)
- Frikha K, Limousy L, Bouaziz J, Bennici S, Chaari K, Jeguirim M. Elaboration of alumina-based materials by solution combustion synthesis: A review. *C. R. Chim*. 2019;22(2–3):206–219. doi:[10.1016/j.crci.2018.10.004](https://doi.org/10.1016/j.crci.2018.10.004)
- Lyagaeva J, Danilov N, Korona D, Farlenkov A, Medvedev D, Demin A, Animitsa I, Tsiakaras P. Improved ceramic and electrical properties of CaZrO₃-based proton-conducting materials prepared by a new convenient combustion synthesis method. *Ceram Int*. 2017;43(9):7184–7192. doi:[10.1016/j.ceramint.2017.03.006](https://doi.org/10.1016/j.ceramint.2017.03.006)
- Khaliullin ShM, Zhuravlev VD, and Bamburov VG. Solution-Combustion Synthesis of MZrO₃ Zirconates (M = Ca, Sr, Ba) in Open Reactor: Thermodynamic Analysis and Experiment. *Int J Self Propag High Temp Synth*. 2017;26(2):93–101. doi:[10.3103/S1061386217020078](https://doi.org/10.3103/S1061386217020078)
- Mukasyan AS, Costello C, Sherlock KP, Lafarga D, Varma A. Perovskite membranes by aqueous combustion synthesis: synthesis and properties. *Sep Purif Technol*. 2001;25(1–3):117–126. doi:[10.1016/S1383-5866\(01\)00096-X](https://doi.org/10.1016/S1383-5866(01)00096-X)
- Zhuravlev V.D., Komolikhov Yu.I., Ermakova L.V. Correlations among sintering temperature, shrinkage, and open porosity of 3.5YSZ/Al₂O₃ composites. *Ceram Int*. 2016;42:8005–8009. doi:[10.1016/j.ceramint.2016.01.204](https://doi.org/10.1016/j.ceramint.2016.01.204)
- Rhodes WH. Agglomerate and particle size effects on sintering yttria-stabilised zirconia. *J Am Ceram Soc*. 1981;64(1):19–22. doi:[10.1111/j.1151-2916.1981.tb09552.x](https://doi.org/10.1111/j.1151-2916.1981.tb09552.x)